International Journal of Heat and Fluid Flow 31 (2010) 101–114

Contents lists available at ScienceDirect

International Journal of Heat and Fluid Flow

journal homepage: www.elsevier.com/locate/ijhff

Modelling bubbly flow and its transitions in vertical annuli using population balance technique

A.K. Das, P.K. Das *

Department of Mechanical Engineering, Indian Institute of Technology Kharagpur, Kharagpur 721302, India

ARTICLE INFO

Article history:
Received 20 July 2009
Received in revised form 18 November 2009
Accepted 23 November 2009
Available online 29 December 2009

Keywords:
Annuli
Bubbly flow
Slug flow
Population balance
Wall peaking
Core peaking

ABSTRACT

Bubbly flow and its transitions in vertical annuli is studied using population balance technique. Bubble breakup and coalescence is accounted separately to track the evolution of the bubble size during the simultaneous flow of gas and liquid. The conventional two-fluid model is used to simulate the hydrodynamics. The model enables the prediction of voidage profile at any axial location. Presence of peak in the void distribution at the walls of the annulus, center of the annulus and both at walls and centers is observed depending on the phase superficial velocities. Further, transition from bubbly to slug and bubbly to dispersed bubbly is predicted based on the evolved bubble size. The model prediction gives a good match with the experimental data and existing theory. A shift in the transition boundary is noted due to the variation in inlet bubble size and the dimension of the annulus.

1. Introduction

Gas liquid two phase flow is observed frequently in diverse engineering systems covering chemical and petroleum processing, oil and gas extraction and transportation, thermal and nuclear power generation etc. In spite of its wide applications two phase flow is one of the least understood domain of fluid dynamics. The two phases can get distributed in a large number of varieties (commonly termed as flow regimes or flow patterns) through any conduit during their motion. This renders the analysis and prediction of flow behavior extremely difficult. For decades scientists and engineers are making tireless efforts to understand two phase flow through experimental investigations (Serizawa et al., 1975; Zun, 1990; Liu and Bankoff, 1993; Liu and Wang, 2001; Lucas et al., 2005) and to model them by developing appropriate theory (Ishii, 1975; Ishii and Mishima, 1984; Drahos et al., 1991; Yeoh and Tu, 2006; Lucas et al., 2007). Most of such endeavors consider two phase flow through circular tubes. The motivation for such a choice emerges from the wide use of circular geometry in engineering applications. Nevertheless, flow through annular passage of circular cross section also occurs frequently. Well bores for the exploration and extraction of oil and natural gas, double pipe heat exchangers, different cooling passages, various gas lift devices are examples where two phase flow occurs through concentric circular annulus. Accordingly, flow of a two phase mixture through annular passage has been investigated by several researchers (Sadatomi et al., 1982; Caetano, 1984; Kelessidis and Dukler, 1989; Hasan and Kabir, 1992; Caetano et al., 1992; Das et al., 1999; Sun et al., 2004).

Sadatomi et al. (1982) studied air water two phase flow through vertical annulus of 15 mm inner diameter and 30 mm outer diameter and determined the average void fraction using quick closing valve technique. They also proposed the transition boundary for bubbly to slug flow. Caetano (1984) investigated air water and air kerosene two phase flow through annuli and observed the transition of bubbly flow to slug flow at a void fraction of 18% and 25% for these two cases respectively. Kelessidis and Dukler (1989) conducted experiments for air water flow in vertical concentric and eccentric annuli of 50.8 mm inner diameter and 76.2 mm outer diameter. They have used probability density function analysis of their conductivity probe signals to identify various flow regimes. Based on this a map has also been introduced for transitions of different flow patterns. Mathematical models based on the physical understanding of different flow patterns have also been developed that matches well with their experimental results.

Hasan and Kabir (1992) studied the effect of annular gap on two phase hydrodynamics using three different annuli. They have used drift flux model to predict average void fraction. Caetano et al. (1992) proposed a transition criterion for bubbly to slug flow using a hydrodynamic model based on eight empirical constants. Their flow pattern map matches well with the data of Hasan and Kabir (1992).

* Corresponding author. Tel.: +91 03222 282916; fax: +91 03222 282278.
E-mail address: pkd@mech.iitkgp.ernet.in (P.K. Das).

0142-727X/$ - see front matter © 2009 Elsevier Inc. All rights reserved.
doi:10.1016/j.ijheatfluidflow.2009.11.006

Nomenclature

a	empirical constant of Eq. (18) (dimensionless)
b	empirical constant of Eq. (18) (dimensionless)
b^*	empirical constant of Eq. (19) (dimensionless)
B	empirical constant of Eq. (9) (dimensionless)
B_B	number of new borne bubbles due to break up (dimensionless)
B_C	number of new borne bubbles due to coalescence (dimensionless)
c_1	constant in Eqs. (15) and (17) (dimensionless)
c_2	empirical constant in Eq. (22) (dimensionless)
c_3	empirical constant in Eq. (23) (dimensionless)
C_D	drag coefficient for a single bubble (dimensionless)
C_{FL}	interfacial friction factor (dimensionless)
d	diameter of the bubbles (m)
d_c	critical bubble diameter for bubble breakup frequency (m)
D	pipe diameter (m)
D_B	number of dying bubbles due to break up (dimensionless)
D_C	number of dying bubbles due to coalescence (dimensionless)
D_{surf}	maximum bubble size possible in dispersed bubbly flow (m)
f	friction factor (dimensionless)
f_{Go}	wall friction factor of gaseous phase (dimensionless)
f_{Lo}	wall friction factor of liquid phase (dimensionless)
f_v	volume fraction of daughter bubble to mother bubble (dimensionless)
F_{LGz}	interfacial force to gaseous phase in axial direction (kg m s^{-2})
F_{LGr}	interfacial force to gaseous phase in radial direction (kg m s^{-2})
F_{dispz}	mass transfer force due to turbulent dispersion in axial direction (kg m s^{-2})
F_{dispr}	mass transfer force due to turbulent dispersion in radial direction (kg m s^{-2})
F_{WGz}	wall gas friction force in axial direction (kg m s^{-2})
F_{WGr}	wall gas friction force in radial direction (kg m s^{-2})
F_{WLz}	wall liquid friction force in axial direction (kg m s^{-2})
F_{WLr}	wall liquid friction force in radial direction (kg m s^{-2})
g_x	gravitational acceleration in x direction (m s^{-2})
$g(a)$	breakage frequency of the bubbles of diameter a (s^{-1})
$h(a, b)$	effective swept volume rate for bubble diameter a and b (s^{-1})
I	normalization coefficient described in Eq. (18) (dimensionless)
k	empirical constant in Eq. (15) (dimensionless)
m	empirical constant of Eq. (19) (dimensionless)
n	empirical constant of Eq. (9) (dimensionless)
$n(r, z, t, d)$	number of bubbles at (r, z) of size d at time t (dimensionless)
$p(a, b)$	film rupture efficiency of bubbles of diameter a and b (dimensionless)
P	pressure of the mixture phase (kg m^{-1} s^{-2})
r	radial direction of the conduit (m)
R_B	average bubble diameter (m)
t	time (s)
U_m	mixture velocity (m s^{-1})
w_g	axial velocity of dispersed phase (m s^{-1})
w_l	axial velocity of continuous phase (m s^{-1})
$v(d)$	volume of the bubble of diameter d (m^3)
u_g	radial velocity of dispersed phase (m s^{-1})
u_l	radial velocity of continuous phase (m s^{-1})
X_c	empirical constant of Eq. (9) (dimensionless)
Y_c	empirical constant of Eq. (9) (dimensionless)
z	axial direction of the conduit (m)

Greek symbols

α	dispersed phase void fraction, (dimensionless)
ΔP_{L0}	single phase frictional pressure drop (kg m^{-1} s^{-2})
ε	energy dissipation rate per unit mass (m^2 s^{-3})
$\eta(a, b)$	daughter bubble probability distribution (dimensionless)
$\lambda(a, b)$	coalescence frequency of bubble diameter a and b (s^{-1})
μ_g	viscosity of discrete phase (kg m^{-1} s^{-1})
μ_l	viscosity of continuous phase (kg m^{-1} s^{-1})
$\nu(a)$	number of bubbles formed from the breakage of a bubble diameter a (dimensionless)
ξ_{min}	non-dimensional minimum daughter bubble size (dimensionless)
ρ_l	density of continuous phase (kg m^{-3})
ρ_g	density of dispersed phase (kg m^{-3})
ρ_m	density of the mixture (kg m^{-3})
σ	surface tension (kg s^{-2})

Das et al. (1999) made experimental observation for air–water upflow through concentric annuli of three different annuli (A: 50.8 mm/25.4 mm, B: 38.1 mm/12.7 mm, C: 25.4 mm/12.7 mm). To identify the distribution of void fraction in different flow regimes parallel plate type conductivity probe was used. Flow regimes were identified using PDF of the signals obtained. Further, they have developed a transition model and compared the model prediction for bubbly to slug flow with different experimental results.

Recently, Sun et al. (2004) observed bubble distribution pattern in their 4.1 m long borosilicate glass tubing of annular cross section. The outer diameter of the tube is 38.1 mm and inner diameter is 19.1 mm. Impedance void meter is used to measure the average void fraction of the test rig. Using the signals obtained from an impedance probe flow patterns have been recognized through a neural network. Their analytical model predicts the transition from bubbly to slug flow at a void fraction of 0.191. Some efforts have also been made for two phase flow through annular conduit in horizontal and inclined orientations. The investigations made by Osamasali and Chang (1988), Ekberg et al. (1999) and Wongwises and Pipathattakul (2006) are worth mentioning.

The review of literature reveals that most of the previous works on two phase flow through annulus are experimental in nature. Time to time some efforts has been made to analyze the flow phenomena through theoretical models. These are primarily phenomenological models developed for specific control volumes based on simplified assumptions. Moreover, in most of the cases these phenomenological models were derived as extensions of the transition criteria previously proposed for circular geometry. Though these models are reasonably successful in predicting the regime boundary they do not provide much insight into the flow behavior at any location or its development along the conduit axis. It is needless to say that a continuum based model which takes care of the spatial and temporal variation of the phase velocities along with the mutual interactions of the phases will not only be able to give a clear picture of the hydrodynamics but will also provide a better prediction of transition.

The direct application of continuum based models of fluid dynamics which are commonly used in case of single phase flow poses some difficulty in case of two phase flow. Further, presence of different regimes in case of two phase flow increases the complexities. To tackle these situations flow regime based models are best suited as the underlying physics behind the regimes are different. Among different types of flow regimes bubbly flow can be described as a homogeneous mixture of gaseous bubble and primary liquid phase. This leads various researchers to model bubbly flow using homogeneous flow model or drift flux model (Zuber and Findlay, 1969). Later on efforts has been made with two-fluid model (Wu et al., 1998; Fu and Ishii, 2003) and population balance model (Yeoh and Tu, 2004; Cheung et al., 2006) to investigate bubbly flow in circular conduit. Though different numerical techniques (Bunner and Tryggvason, 2002) are employed to simulate bubble evolution in circular tube, population balance technique coupled with two-fluid model emerges as an effective and robust technique (Cheung et al., 2006; Das et al., 2009a,b; Yeoh and Tu, 2004) for predicting interfacial behavior in bubbly flow. Unfortunately, not much effort has been made to simulate bubbly flow and its transition in an annulus through computational approach.

In the present work a Eulerian–Eulerian two-fluid model have been used to simulate bubbly flow through the annuli. A Lagrangian population balance technique has been super imposed in the model to track the evolution of the bubbles due to breakup and coalescence. A criteria based on maximum bubble diameter has been chosen to predict bubbly to slug transition. The model prediction shows excellent agreement with the available experimental results and theory. Further studies have been done to find out the voidage profile in bubbly flow and different peaked structures depending on the phase superficial velocities. Effect of bubble size at the inlet of the conduit and the annular spacing on transition boundary has been investigated. The transition from bubbly to dispersed bubbly flow has also been predicted and validated against the available experimental data.

2. Model development

The flow phenomena simulated in the present work is schematically shown in Fig. 1. Present model is developed in two parts. Initially, basic flow field of gas and liquid is obtained using axisymmetric two-fluid model. Next, the population balance technique is used to determine the evolution of bubble size and distribution through the process of coalescence and break up. In this stage the spatial velocity of the phases has been used as the input. Following assumptions has been made for the model development:

(i) The two fluids are incompressible and Newtonian.
(ii) Properties of fluids are uniform and constant.
(iii) Bubbles are spherical in shape having diameter as the characteristic length.
(iv) Isotropic turbulence is considered for calculating the turbulence intensity and the eddy size. Turbulence properties are linked with mean flow velocities to close the system of equations.
(v) Bubble breakage and coalescence is taken as the only source term in the population balance equation. Deformation, growth shrinkage, nucleation and condensation are not considered in the present model.
(vi) Binary breakage and coalescence is considered.

Other assumptions are described in the models wherever necessary.

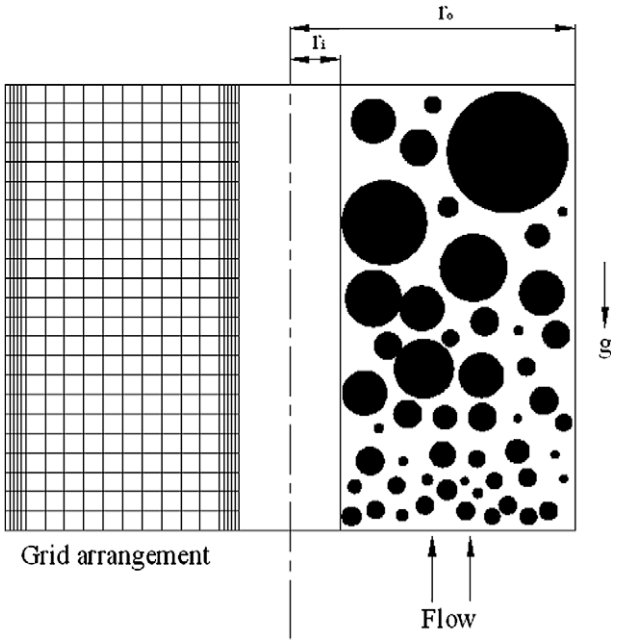

Fig. 1. Bubble distribution and grid arrangement in annuli filled with air water bubbly flow.

2.1. Two-fluid model

In the two-fluid model (Anderson and Jackson, 1967) it is assumed that two phase flow consists of two individual single phase flows. Contribution of each of the phases is considered introducing respective phase fractions. Two set of conservation equation similar to single phase flow system is used with appropriate correlations for interfacial interactions. Such interactions are cumulative as bubbles are not individually tracked in an Eulerian–Eulerian approach of modeling.

2.1.1. Continuity equation

In the absence of mass transfer between the two phases the mass conservation equations can be written for each of the phases as follows:

Gas phase:

$$\frac{\partial}{\partial t}[\rho_1(1-\alpha)] + \frac{1}{r}\frac{\partial}{\partial r}[r\rho_1(1-\alpha)u_1] + \frac{\partial}{\partial z}[\rho_1(1-\alpha)w_1] = 0 \quad (1)$$

Liquid phase:

$$\frac{\partial}{\partial t}[\rho_g\alpha] + \frac{1}{r}\frac{\partial}{\partial r}[r\rho_g\alpha u_g] + \frac{\partial}{\partial z}[\rho_g\alpha w_g] = 0 \quad (2)$$

Here α signifies the phase fraction of the gaseous phase and $(1-\alpha)$ gives the phase fraction of the liquid phase. Subscripts l, g denotes liquid and gas phase respectively.

2.1.2. Momentum conservation

The temporal and the spatial averaging of the fluid properties has been made for the derivation of momentum equation. As the macroscopic field of one phase is not independent of the other, the interaction terms of each phase across the interface appears in the field equation of the momentum conservation (Frank et al., 2004). Along with the interfacial forces, force due to interaction with the solid wall needs to be taken care of using appropriate closure equations. The momentum equation of the two phases can be written as follows:

Gas phase:

r momentum:

$$\frac{\partial}{\partial t}[\rho_g \alpha u_g] + \frac{\partial}{\partial r}[\rho_g \alpha u_g^2] + \frac{\partial}{\partial z}[\rho_g \alpha u_g w_g] = -\alpha \frac{\partial P}{\partial r} + \alpha \rho_g g_r + \mu_g \frac{\partial^2}{\partial r^2}(\alpha u_g) + \frac{\mu_g \alpha u_g}{r^2} + \frac{\mu_g}{r}\frac{\partial}{\partial r}(\alpha u_g) + \mu_g \frac{\partial^2}{\partial z^2}(\alpha u_g) - F_{WGr} - F_{LGr} - F_{dispr} \quad (3)$$

z momentum:

$$\frac{\partial}{\partial t}[\rho_g \alpha w_g] + \frac{\partial}{\partial r}[\rho_g \alpha u_g w_g] + \frac{\partial}{\partial z}[\rho_g \alpha w_g^2] = -\alpha \frac{\partial P}{\partial z} + \alpha \rho_g g_z + \mu_g \frac{\partial^2}{\partial r^2}(\alpha w_g) + \frac{\mu_g}{r}\frac{\partial}{\partial r}(\alpha w_g) + \mu_g \frac{\partial^2}{\partial z^2}(\alpha w_g) - F_{WGz} - F_{LGz} - F_{dispz} \quad (4)$$

Liquid phase:
r momentum:

$$\frac{\partial}{\partial t}[\rho_1(1-\alpha)u_1] + \frac{\partial}{\partial r}[\rho_1(1-\alpha)u_1^2] + \frac{\partial}{\partial Z}[\rho_1(1-\alpha)u_1 w_1] = -(1-\alpha)\frac{\partial p}{\partial r} + (1-\alpha)\rho_1 g_r + \mu_1 \frac{\partial^2}{\partial r^2}((1-\alpha)u_1) + \frac{\mu_1(1-\alpha)u_1}{r^2} + \frac{\mu_1}{r}\frac{\partial}{\partial r}((1-\alpha)u_1) + \mu_1 \frac{\partial^2}{\partial z^2}((1-\alpha)u_1) - F_{WLr} - F_{LLz} + F_{dispz} \quad (5)$$

z momentum:

$$\frac{\partial}{\partial t}[\rho_1(1-\alpha)w_1] + \frac{\partial}{\partial r}[\rho_1(1-\alpha)u_1 w_1] + \frac{\partial}{\partial Z}[\rho_1(1-\alpha)w_1^2] = -(1-\alpha)\frac{\partial p}{\partial z} + (1-\alpha)\rho_1 g_z + \frac{\mu_1}{r}\frac{\partial}{\partial r}((1-\alpha)w_1) + \mu_1 \frac{\partial^2}{\partial r^2} \times ((1-\alpha)w_1) + \mu_1 \frac{\partial^2}{\partial z^2}((1-\alpha)w_1) - F_{WLz} - F_{LLz} + F_{dispz} \quad (6)$$

P is assumed as the average pressure of the mixture and it can be evaluated using the equation of state in the following manner:

$$P = (\rho_l \alpha_l + \rho_g \alpha_g)RT \quad (7)$$

Forces due to wall lubrication, interfacial forces to the liquid and gaseous phases are described in the next section.

2.1.3. Interfacial momentum transfer

Interfacial forces which affect the hydrodynamics are the drag force, the virtual mass force, the transverse lift force and the turbulence dispersion force. Among these, drag force has the major influence over the development of the flow field in vertical upflow. Lateral lift force is also a prime interfacial force for gas liquid two phase flow. Tomiyama et al. (2003) proposed lateral lift coefficient based on bubble sizes. In the present model this force has not been considered. Incorporation of such force is expected to improve the prediction. This clearly leaves a scope for further improvement of the present model.

As the generic nature of the radial and axial forces is same, directions of the forces are omitted in the respective equations. For the vector quantities associated with the forces we have used their non-directional forms by putting a bar over the symbols of the respective vectors. For the directional equation of the forces the quantities under the bar will be substituted by the respective directional form of the vectors. For the flow of discrete bubbles in a continuous medium some simplification can be made to club the major interfacial forces. Following the development of Richter (1983) the net interfacial force can be taken as:

$$\overline{F_{LG}} = \frac{2C_{FL}}{D}\sqrt{\alpha}\rho_g(\overline{u_g} - \overline{u_l})|\overline{u_g} - \overline{u_l}| + \frac{\alpha}{2}\rho_1 \overline{u_g}\frac{\partial}{\partial_r}(\overline{u_g} - \overline{u_l}) \quad (8)$$

In the above expression C_{FL} is interfacial friction factor which includes a modified relationship for drag in a two phase medium.

$$C_{FL} = C_D\sqrt{\alpha}(1-\alpha)^{-1.7}\frac{\rho_1}{\rho_g}\frac{D}{2R_B} \quad (9)$$

where R_B is average bubble radius and C_D is drag coefficient for a single bubble. Eq. (9) needs the information of bubble diameter which is determined in the present work through population balance.

F_{WL} in Eqs. (5) and (6) is the wall liquid friction force. Based on Chisholm's (1973) correlation it can be written as follows:

$$F_{wL} = \left[1 + (Y_c^2 - 1)\left(B(X_c(1-X_c))^{\frac{2-n}{2}} + X_c^{2-n}\right)\right]\Delta P_{L0} \quad (10)$$

Here ΔP_{L0} is the single phase friction pressure drop, B is an empirical constant dependent on the fluid pair and $n = 0.25$ for air water system. X_c and Y_c can be expressed as follows:

$$X_c = \frac{1}{1 + \frac{1-\alpha}{\alpha}\frac{\rho_l}{\rho_g}\frac{\overline{u_l}}{\overline{u_g}}} \quad \text{and} \quad Y_c = \left(\frac{f_{Go}\rho_l}{f_{Lo}\rho_g}\right)^{0.5} \quad (11)$$

Wall friction factor of gaseous phase is also calculated in the same manner.

The turbulent dispersion force of gaseous phase (Lopez de Bertodano, 1998) is considered in the form of Favre averaged variables.

$$F_{disp} = C_{ID}C_D\frac{y_{tg}}{Sc_{tg}}\left[\frac{\nabla\alpha_l}{\alpha_l} - \frac{\nabla\alpha_g}{\alpha_g}\right] \quad (12)$$

C_{TD} and C_D are the turbulent dispersion force coefficient and the Drag force coefficient for a single bubble. C_{TD} is taken as 1.0 in the present simulation. γ_{tg} is the turbulence kinetic viscosity and Sc_{tg} is the turbulent Schmidt number of the gaseous phase.

2.2. Population balance equation

To keep a track of the bubble kinetics a population balance (Kumar and Ramkrishna, 1996) equation has been incorporated in the present model. As interactions of a large number of bubbles of various sizes are present, tracking the bubble population is necessary to determine the dynamics of bubble evolution through coalescence and breakage. Birth and death of bubbles due to breakage and coalescence depend on the transport properties and velocities of neighboring continuous phase. The birth and death of bubbles are cumulative functions of the entire population. So an interrelated integral–differential equation must be tackled numerically to resolve the characteristics of the individual bubbles.

The population balance equation can be expressed in the following generalized form:

$$\frac{\partial n(r,z,t,d)}{\partial t} + u_g\frac{\partial n(r,z,t,d)}{\partial r} + w_g\frac{\partial n(r,z,t,d)}{\partial z} = B_B(r,z,t,d) - D_B(r,z,t,d) + B_c(r,z,t,d) - D_c(r,z,t,d) \quad (13)$$

In the present model above equation is discretized in order to solve it with the usual grid based technique keeping internal consistency with regard to the second order moment of distribution (Kumar and Ramkrishna, 1996). Discretization of the bubble population into different subgroup has been done based on uniform volume intervals and bubbles of any size other than the pivotal sizes, formed due to bubble breakage, are distributed among the neigh-

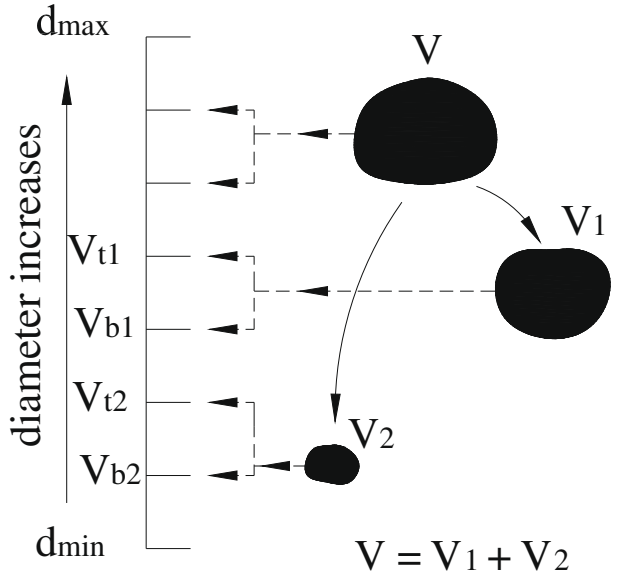

Fig. 2. Scheme of redistribution of daughter bubbles, generated due to breakage, into their immediate neighbors.

boring sizes keeping the bubble mass and number fixed. The scheme of redistribution of the daughter bubbles is shown in Fig. 2. Following conditions are satisfied during the redistribution:

$$\text{for} \quad i = 1 \text{ and } 2 \quad V_i = n_{bi}V_{bi} + n_{ti}V_{ti} \;\&\; n_{bi} + n_{ti} = 1 \tag{14}$$

Present model only recognizes the appearance or disappearance of the newly born or dead particles in a fixed control volume. However, their redistribution is considered as random and solely guided by the convection of mixture phase. Present model is developed only for binary coalescence and binary breakage of the bubble.

2.2.1. Break up process

Following the concept of classical statistical approach of isotropic turbulence the two phase mixture is assumed to be an assemblage of eddies having their respective kinematics. Each eddy is characterized by its size and energy (Kostoglou and Karabelas, 1998). Due to the collision with these turbulent eddies fragmentation of bubbles takes place. Breakage of a bubble is possible only when the turbulent kinetic energy of the striking eddy supply the surface energy needed for the process. If the eddy size is larger than the bubble characteristic length it is assumed that the interaction between them is unable to make any large deformation of the bubble shape which can ultimately result into a breakage. This type of collision only causes the transport of the bubble in the flow field. Sizes of the daughter bubbles due to the collision of eddy and bubbles depend on the strength of the eddy (Luo and Svendsen, 1996). But the collision frequency between them is solely guided by the transport properties of the flow field. It is also assumed that size and strength of eddies do not alter as a result of collision with the bubbles. Further, it is assumed that the daughter bubbles achieve a spherical shape instantaneously after its birth from its predecessor.

Birth and death of bubbles due to breakup process can be calculated as follows:

$$B_B(r,z,t,d) = \int_d^\infty \eta(d'-d,d)\,v(d')g(d')n(r,z,t,d')dd' \tag{15}$$

$$D_B(r,z,t,d) = n(r,z,t,d)g(d) \tag{16}$$

Here $\eta(d_1, d_2)$ is the daughter probability distribution $(1/m)$ for the breakage of a bubble of diameter $d_1 + d_2$. $v(d)$ is the number of bubbles formed from the breakage of a bubble diameter d. $g(d)$ is the breakage frequency of the bubbles of diameter d (1/s). $\eta(r, z, t, d)$ is the number density of a particular bubble diameter d at a fixed coordinate (r, z) at any instant t.

The strength of the colliding eddy must be greater than the surface energy of the bigger bubbles created by breakage event. Similarly, according to the capillary pressure formulation (Wang et al., 2003) the dynamic pressure of the turbulent eddy must be larger than the capillary pressure of the smaller fragment of breakup. Successful separation of the two bubbles depends on the contact time of eddy and bubble which should be sufficient for drainage or rupture of the intervening film between them. Based on the model proposed by Kostoglou and Karabelas (2006) bubble breakup frequency can be expressed as:

$$g(d) = k(1-\alpha)\left(\frac{\epsilon}{d^2}\right)^{\frac{1}{3}}\int_0^1\int_{\xi_{\min}}^1 \frac{(1+\xi)^2}{\xi^{\frac{11}{3}}} e^{\left(-\frac{12c_1\sigma}{2.04\rho_c\epsilon^{\frac{2}{3}}d^{\frac{5}{3}}\epsilon^{\frac{11}{3}}}\right)} d\epsilon df_v \tag{17}$$

Here f_v is the ratio of the volume of mother and daughter bubbles and ε is the energy dissipation rate per unit mass. ε can be estimated (Ioannou et al., 2004) in terms of pipe diameter (D) and mixture velocity (U_m):

$$\varepsilon = \frac{fU_m^3}{2D} \tag{18}$$

U_m is calculated as follows:

$$U_m = \sqrt{(u_g^2 + w_g^2)^2} + \sqrt{(u_l^2 + w_l^2)^2} \tag{19}$$

C_1 is an empirical constant and can be expressed in terms of f_v as follows:

$$C_1 = f_v^{\frac{2}{3}} + (1-f_v)^{\frac{2}{3}} - 1 \tag{20}$$

$\xi_{\min}$ is the non-dimensional minimum daughter bubble size that can be obtained from the Kolmogroff microscale as described by Tsouris and Tavlarides (1994). Daughter distribution probability presented by Kostoglou and Karabelas (1998) is used in the present model. Based on their theory the probability of size distribution of daughter drops can be expressed as follows:

$$\eta(d_1,d_2) = \left(\frac{1}{\frac{d_1}{d_2}+a} + \frac{1}{1-\frac{d_1}{d_2}+b} + \frac{2(z-1)}{b+0.5}\right)\frac{6I}{\pi d_2^3} \tag{21}$$

where I is the normalization coefficient and expressed as:

$$L = \frac{0.5}{\ln(l+a) - \ln(b) + \frac{z-1}{b+0.5}} \quad \text{and} \quad Z = \frac{a}{4b(l+b)(l-a)}$$

a and b are parameters that define the shape of the daughter drop size distribution function. In the present model the values $a = 0.1$ and $b = 1$ are used. This signifies "U" shaped bubble size distribution (Kostoglou et al., 1997).

A bubble of size larger than a critical value will break up quickly because of the instability of the liquid gas interface. The following empirical equation was used by Carrica and Clausse (1993) to calculate the bubble breakup rate due to instability:

$$g(d) = b^* \frac{(d-d_c)^m}{(d-d_c)^m + d_c^m} \tag{22}$$

where d_c is the critical bubble diameter set as 27 mm for air water system as followed by Carrica and Clausse (1993). b^* and m are model parameters and were set as 100 (1/s) and 6.0, respectively.

2.2.2. Coalescence process

For coalescence of bubbles to occur in a turbulent flow field of a two fluid mixture the bubbles must first collide with each other

and then remain in contact for a sufficient time so that the processes of liquid film drainage, film rupture and finally coalescence may occur (Coulaloglou and Tavlarides, 1977). During these processes a turbulent eddy may separate the droplets and prevent coalescence. To close the uncertain coalescence model maximum particle volume, bubble collision frequency and bubble coalescence efficiency are required.

Three main mechanisms of bubble coalescence in a gas–liquid system exist: (1) coalescence resulting from turbulent eddies, (2) coalescence resulting from different rise velocities (buoyancy) (Fu and Ishii, 2003) and (3) coalescence resulting from bubble wake entrainment (Prince and Blanch, 1990). Nevertheless, in most of the situations the influence of turbulent eddies over the coalescence process is dominant. The following expressions can be used for the process of birth and death respectively due to coalescence:

$$B_c(r,z,t,d) = \frac{1}{2}\int_0^{v(d)/2} \lambda(d_{v-v',d_v}) n(r,z,t,d_{v-v'}) n(r,z,t,d_{v'}) dv' \quad (23)$$

$$D_c(r,z,t,d) = n(r,z,t,d_v)\int_0^{\infty} \lambda(d_v,d_{v'}) n(r,z,t,d_{v'}) dv' \quad (24)$$

Here $\lambda(d_1, d_2)$ is the coalescence frequency of bubble diameter d_1 and d_2.

Details of coalescence process are described elsewhere (Das et al., 2009a,b). The probability for a collision to result in coalescence is termed as coalescence efficiency. During all these processes if the pair strikes with another eddy of sufficient strength the coalescence process may terminate at any time without fusing them.

Coalescence frequency $\lambda(d_1, d_2)$ is the product of the effective swept volume rate, $h(d_1, d_2)$ and film rupture efficiency $p(d_1, d_2)$. Effective swept volume rate is calculated using the analogy between kinetic theory of gasses and bubble coalescence phenomena. According to Coulaloglou and Tavlarides (1977) effective swept volume rate can be calculated as:

$$h(d_1,d_2) = c_2 \frac{\varepsilon}{1+\alpha}(d_1+d_2)^2\left(d_1^{\frac{2}{3}}+d_2^{\frac{2}{3}}\right)^{\frac{1}{2}} \quad (25)$$

Film rupture efficiency can be calculated using the exponential function of the ratio of liquid film drainage time to drop contact time. The bubbles have to be in contact for a certain period of time, sufficient for the liquid film to reach the critical thickness. Effect of Van der Waal's force and force of electric double layer which can retard the film drainage is neglected. Coalescence time is estimated only as the time required for the film drainage between the bubbles. If the bubbles are separated by an incoming eddy before the proposed thickness is reached, no coalescence occurs. Film drainage is controlled by inertia and surface tension forces (Chesters, 1991). For two bubbles of diameter d_1 and d_2 Coulaloglou and Tavlarides (1977) proposed the film rupture efficiency is as follows:

$$P(d_1,d_2) = \exp\left[-\frac{c_3\rho_l\mu_l\varepsilon}{\sigma^2(1+\alpha)^3}\left(\frac{d_1d_2}{d_1+d_2}\right)^4\right] \quad (26)$$

Two case dependent numerical constants (c_2 and c_3) are associated with coalescence rate function. c_2 is related to the collision frequency and c_3 is related to the rupture efficiency. Further, these coefficients also depend on the minimum film thickness h_0, instantaneous film thickness h, and some other (Coulaloglou and Tavlarides, 1977) dimensionless constants associated with equations expressing the contact time of two drops, the force compressing two drops together, and the energy properties of the turbulent field.

Values of c_2 and c_3 are taken as $0.0055\phi^{-1.3404}$ and 5.4×10^8 as suggested by Ioannou et al. (2004). They used the experimental data of Lovick (2004) to fit the values of the above constants.

2.3. Boundary conditions and solution procedure

Following boundary conditions are employed to simulate the flow of a gas liquid mixture through annuli:

i Both the phases have uniform velocity profile in the stream wise direction and zero velocity in the crosswise direction.
ii No slip and no penetration conditions are imposed at the walls.
iii Inlet void fraction (α) is taken as an input to the system of Eqs. (1)–(6).

For the proper impositions of the no slip boundary conditions finer grids have been adopted at the wall. Further, a small velocity as per the logarithmic law (Lienhard and Lienhard, 2004) of buffer layer is implemented at a very small distance from the conduit wall.

In the population balance model initial condition for the bubble size distribution is taken as:

$$n(r,z,0,d) = 0 \quad (27)$$

And inlet boundary condition is taken as:

$$\begin{aligned} n(0,z,t,d) &= n(r,d) \\ P(0,z,t) &= \text{const.} \end{aligned} \quad (28)$$

In the present work uniform distribution of bubbles at the inlet is assumed. This simulates the experimental condition where the dispersed phase is introduced at the inlet of the test section through a large number of nozzles of uniform diameter or through a fixed bed of porous material (Eckert et al., 2003). Pressure at inlet and outlet boundary is considered as atmospheric. At the inner and outer wall of the pipe, gradient of all the variables are taken as zero obeying no slip and no penetration condition. Overall possible bubble sizes are divided into 40 equal volume based group to consider the possibility of a varied distribution of air bubbles. Properties of purified water and air at 27 °C are used for the mixture of two phase flow.

Solving Eqs. (1)–(6) velocity field at each grid point is calculated and the mixture velocity at that particular position is determined. Mixture velocity is used to determine the distribution of bubble size for the next instant based on the population balance equation (Eq. (13)). Simulation is forward marched and the development of flow along the down stream is closely monitored. There may be several outcomes depending on the operating conditions. At a sufficient length away from the inlet plane a statistically stable bubble distribution (with respect to bubble size and number) may be obtained. This indicates steady bubbly flow. On the other hand, one may observe continuous increase in the bubble size due to coalescence. Eventually such a situation leads to slug flow. As the present model is developed specifically for bubbly flow it cannot be used to simulate slug flow. However, one may detect the inception of slug flow by tracking the growth in the bubble size. Bubbly flow can terminate into slug flow if the maximum bubble size exceeds a certain limit. Various researchers proposed various limits for transition in terms of a critical bubble diameter. Tomiyama et al. (2003) considers a bubble to be a slug bubble when its equivalent diameter is 0.6 of tube diameter. Krussenberg et al. (1999) and Lucas et al. (2005) also suggest a differentiation between bubbly flow and slug flow based on the equivalent diameter of the largest bubble. Taking the queue from the above studies the criterion for bubbly to slug transition has been set for the present study to terminate the simulation. Maximum bubble diameter in case of bubbly flow crossing the half of the annular spacing is the inception of slug flow.

3. Results and discussions

Gas liquid flow through an annular cross section is solved using 2D axisymmetric grids in a cylindrical polar coordinate system. To check the grid-independence of the solution, the influence of the number of radial grids on the numerical simulation is studied. The grid structure used in the present paper is non-uniform, with finer mesh close to the inner and outer walls, as shown in Fig. 1. The results for the radial profiles of the void fraction at air velocity of 1 m/s and water velocity of 3 m/s for 30, 40 and 50 radial grids are depicted in Fig. 3. There is no perceptible difference between the results using 40 radial grids and 50 radial grids; therefore 40 grids were used for all simulations in this work. Present model is used to predict the transition of bubbly flow through the annuli. For co-current upflow with the change of phase superficial velocity, bubbly flow transforms either into slug flow or into dispersed bubbly flow (Wallis, 1969). Therefore in the present work efforts have been made to determine the boundaries of these two transitions.

3.1. Validation of the developed model

At first the developed model is validated with the reported radial void distribution from literature. Air and water at atmospheric pressure and at a temperature of 25 °C are considered as the two phases for the simulation of bubbly flow. Inlet bubble diameter is kept as 0.05 times of the annular spacing. With 40 radial grids and 100 axial grids simulations have been made for prediction of radial void distribution. In Fig. 4a the present model is validated with a core peaking void distribution pattern as reported by Sorour and El-Beshbeeshy (1986). They have used electrical resistivity probe to measure the radial void distribution pattern for annuli having 38 mm inner and 75 mm outer diameter. Present model is simulated for the same flow conditions and void distribution pattern is reported at an axial distance of 43.5 times of the annular spacing. It can be observed from the figure that the result of the present model matches very well with the core peaked void distribution reported in the literature.

Efforts have also made to examine the predictability of the model for situations where bubbles are pushed towards the walls of the annuli showing two wall peaks. Present model is used to predict the void distribution pattern for bubbly flow inside annuli having 38.1 mm outer diameter and 19.1 mm inner diameter. Hibiki et al. (2003) performed experimental investigation on similar situations and reported void distribution pattern at a radial plane 51 times of the annular spacing away from the inlet. They have

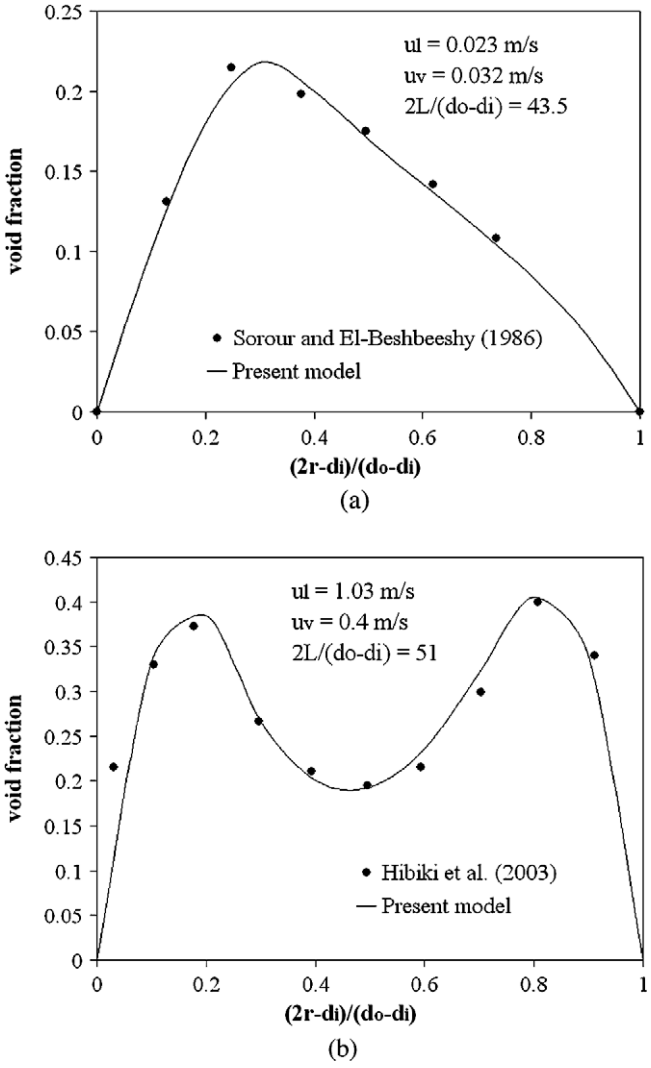

Fig. 4. Prediction of radial void distribution pattern for bubbly flow inside annuli.

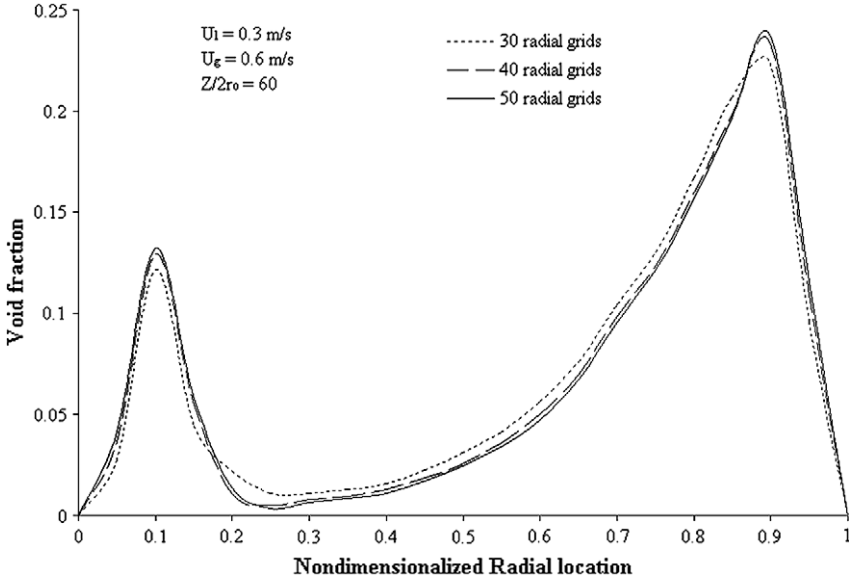

Fig. 3. Effect of radial mesh refinement on void distribution.

used double sensor conductivity probe to measure the instantaneous radial pattern of void distribution. Results of the present numerical simulation and experimental data reported by Hibiki et al. (2003) are reported in Fig. 4b for comparison. It can be observed from the figure that present model also predicts the gathering of bubbles near both the wall efficiently.

3.2. Bubbly to slug transition

Next, simulations have been done for a fixed water flow rate varying the air flow rate until the criteria for transition from bubbly to slug flow is met. The flow velocities of air and water at which bubbly flow pattern changes to slug flow is plotted in the flow pattern map. Next, water flow rate is changed in step and same procedures are followed to obtain the next point of the flow pattern map. Based on the local turbulent dissipation rate (ε) and average bubble diameter, breakage or coalescence of bubbles occurs at each grid in the annuli. If the coalescence is encouraged bigger bubbles form and they move towards the centre of the annuli showing the core peaking pattern before the slug flow regime. For a comparison of the estimated transition boundary with the available experimental results, observation of Caetano (1984) and Kelessidis and Dukler (1989) is plotted in the Fig. 5. It can be seen from the figure that the computed result at $60X(r_0 - r_i)$ is matching well with experimental observation of Caetano (1984). But observation of Kelessidis and Dukler (1989) is over predicted by the present model. It may be noted that certain amount of subjectivity is associated with the prediction of flow regime boundary in any experiment. Therefore, the mismatch observed in two experimental results (Fig. 5) is not surprising. However, the annular gap of the test section used by Kelessidis and Dukler (1989) is 25.4 mm which is half of that used by Caetano (1984). This may have some effect on the transition of flow regimes. Further, experimental verifications are needed to ascertain this.

Comparison of the present simulation was also made with other theoretical flow pattern transition criteria available in literature. Transition map of bubbly flow to slug flow presented by Das et al. (1999) and Sun et al. (2004) is depicted in the same figure. All the predictions follow the same trend as shown by the present model. Das et al. (1999) and Sun et al. (2004) matches well with experimental observations of Kelessidis and Dukler (1989) but under predicts the experimental observations of Caetano (1984). Though the agreement of the present model with the data from the narrow annuli is not excellent the concordance of the present model and the published theoretical maps is still satisfactory. Transition model for bubbly to slug flow in circular tube presented by Mishima and Ishii (1984) is also plotted in Fig. 5 as a benchmark. All the transition boundaries exhibit the same trend depicted by the Mishima and Ishii (1984) model. It essentially signifies identical physical phenomena responsible for the transition of bubbly to slug flow in both the geometries. The influence of geometry is manifested in the shift between the transition boundaries of the annuli and the circular tube.

The macroscopic nature of the population balance equation of the present model allows probing into the distribution of local void fraction. Simulations were made for various air and water flow rates through an annulus of 50 mm outer diameter and 20 mm inner diameter. Diameter of the bubbles at the inlet is kept at 1.5 mm. It has been observed that the void distribution pattern changes with the change in superficial flow velocities. Distribution of gaseous phase at various superficial flow velocities are depicted in Fig. 6a. At low air and water flow rates bubbles entering into the annulus try to shift towards the outer wall. Result for 0.3 m/s water velocity and 0.1 m/s air velocity shows a sharp peak in the void distribution profile at the outer wall of the annular geometry. With the increase of gas flow rate some bubbles move towards the inner wall while most of them continue to stick with the outer wall of the annulus. As a result a secondary peak in the void distribution pattern can be seen near the inner wall along with the dominant

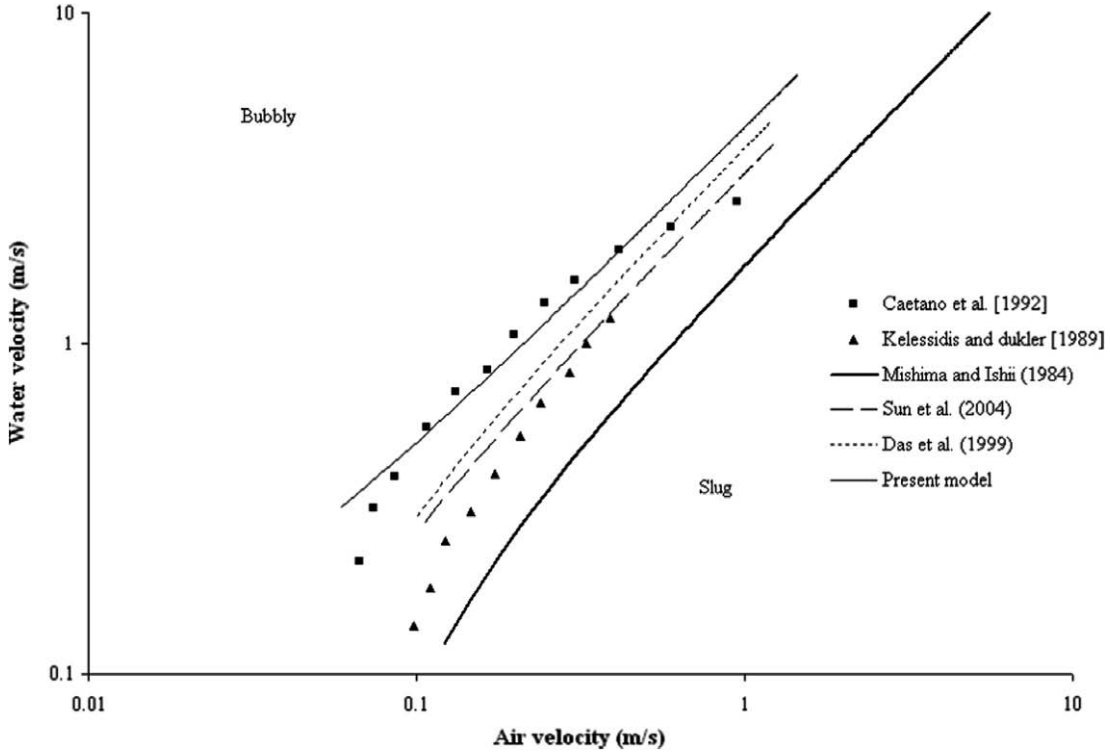

Fig. 5. Bubbly-slug transition map for air water two phase flow through annuli along with available experimental and theoretical results.

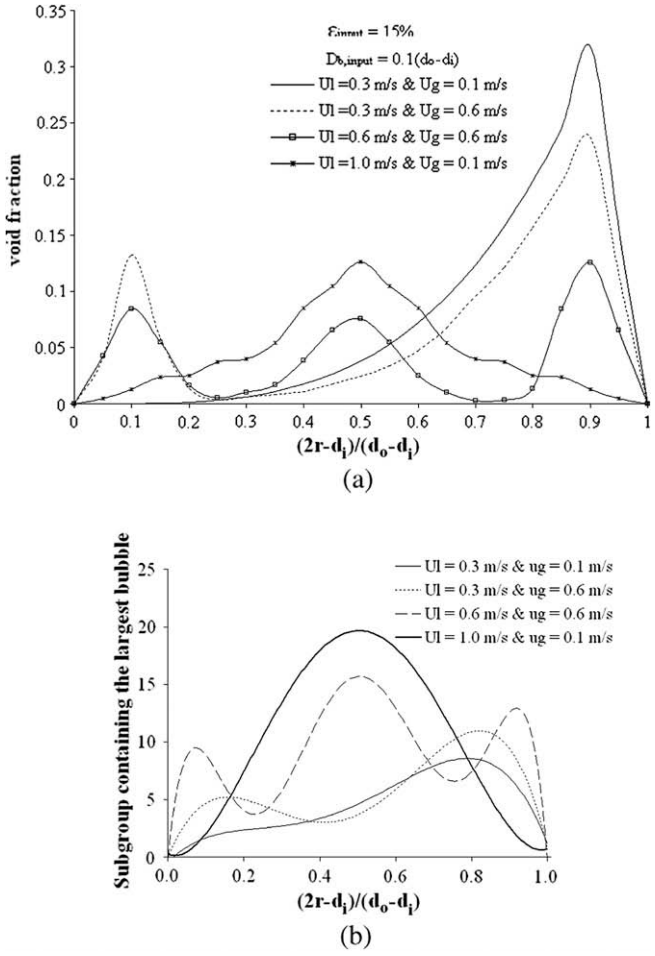

Fig. 6. Various shapes of void and bubble distribution pattern in a radial plane for different superficial velocities of air and water.

peak at the outer wall. One example of such type of distribution is plotted in Fig. 6a for liquid and air velocities of 0.3 m/s and 0.6 m/s respectively. Further increase in liquid velocity forces the bubbles to move through the core of the annuli due to the increased vibration induced by turbulence. As a result, at a liquid velocity of 0.6 m/s and gas velocity 0.6 m/s a third peak at the core of the annular gap can be observed. It may be noted that the peaks at the walls are lowered with the appearance of a new peak at the center of the annulus. At high liquid flow rate the tendency of a bubble to shift towards the core increases. As a result a single dominant peak at the center of the annular gap is observed. In Fig. 6a void distribution pattern for liquid flow rate of 1 m/s and gas flow rate of 0.1 m/s shows similar kind of phenomena. From this distribution it is clear that most of the bubbles concentrate in the central region of the annular spacing at high liquid superficial velocities. Largest bubble size present in the control volumes along the radial plane is also depicted in Fig. 6b for the above mentioned combinations of liquid and gaseous phase velocities. It can be observed from the figure that as a dominant peak is observed near the wall (peak at outer wall and peak at both walls) largest possible bubble size near the wall decreases. On the other hand the peak of void distribution at the center of the annuli is generated due to comparatively bigger sized bubbles.

At a particular liquid and gas velocity if the mixture velocities are conducive for smaller bubbles, predominantly breakage of bigger bubbles occurs. Due to the presence of large numbers of smaller sized bubbles average diameter of bubbles at a control volume reduces. Smaller average bubble diameter generates higher interfacial forces which dominate over the wall force. This helps the bubbles at the centre of the tube to move towards the wall. As a result wall peaking void distribution pattern is generated.

On the other hand, at other phase velocities which support coalescence, bigger bubbles are generated. Due to the increase of average bubble diameter inside the tube, interfacial forces decrease. This makes the wall force to dominate and the bubbles tend to crowd towards the core. Core peaking can be observed due to the accumulation of big bubbles at the tube centre. At some intermediate velocities of the phases when both breakage and coalescence are significant, big bubbles are gathered at the tube centre and smaller bubbles at the wall. As a result a two peaked structure can be observed.

From the above exercise it is clear that the radial voidage distribution vary substantially depending on the operating conditions. Further, one mode of voidage distribution may change into another. In Fig. 7 four well demarcated regimes has been shown inside the bubbly flow pattern where outer wall peaking, both wall peaking, three peak and core peak can be viewed prominently. The simulation is for an input bubble diameter of 1.5 mm inside a 30 mm annular spacing with 20 mm inner radius. It may be appreciated that before the transition into slug flow regime, the bubbles tend to gather at the core of the annuli. This causes coalescence of the bubbles. Coalescence of the spheroidal bubbles produces cap bubbles which in turn grows to form gas slugs and signifies the inception of slug flow. On the other hand, at a relatively high water flow rate as coalescence is prevented bubbly flow terminates into dispersed bubbly flow. The mechanism of this transition has been discussed in a later section.

3.3. Influence of input parameters

In the present model coalescence and break up are the only mechanisms behind the change in bubble size. Diameter of inlet bubble also influences the evolution of bubble size further downstream. Studies have been made for different homogeneous and non-homogeneous input of bubbles at the inlet plane. Fig. 8a depicts the void fraction profile for two different input diameters of bubbles inside the annular passage (ID = 20 mm, OD = 50 mm) for a liquid velocity of 0.3 m/s and air velocity of 0.6 m/s. The void fraction profiles are computed at 30*D* from the inlet plane to avoid entrance effect. Dominant peaks at the walls in the void distribution profile can be seen for bubbles of 2 mm diameter. For such small bubbles interfacial forces dominate over the effect of wall force. Wall force becomes comparable to the decreased interfacial forces when bubbles of 4 mm diameter are introduced at the inlet plane for same flow velocities. Strong core peaking can be viewed in this case. Simulation has also been made for simultaneous entry of 2 mm and 4 mm bubbles at the inlet plane keeping the inlet void fraction constant. The figure depicts three peak distributions as the hydrodynamics is influenced by the individual behavior of both the sizes. It can be easily understood that 4 mm bubbles crowd towards the core of the annuli while 2 mm bubbles tends to move towards the wall of the annuli. Largest bubble sizes in the radial control volumes are also depicted in Fig. 8b for the following sizes of bubble diameter at the entry – 2 mm, 4 mm and an equal mixture of 2 mm and 4 mm bubbles by volume. It can be observed from the figure that the largest possible bubble size for the 4 mm bubbles at the entry is higher compared to that when 2 mm bubbles enter at the inlet. This also confirms the core peaking for the bigger bubbles and wall peaking for smaller bubbles. For simultaneous entry of 2 mm and 4 mm sized bubbles, bubbles of bigger diameter are observed at the core as well as both at the inner and the outer walls.

Influence of inlet bubble size on flow pattern map has also been studied using the present population balance technique. In Fig. 9

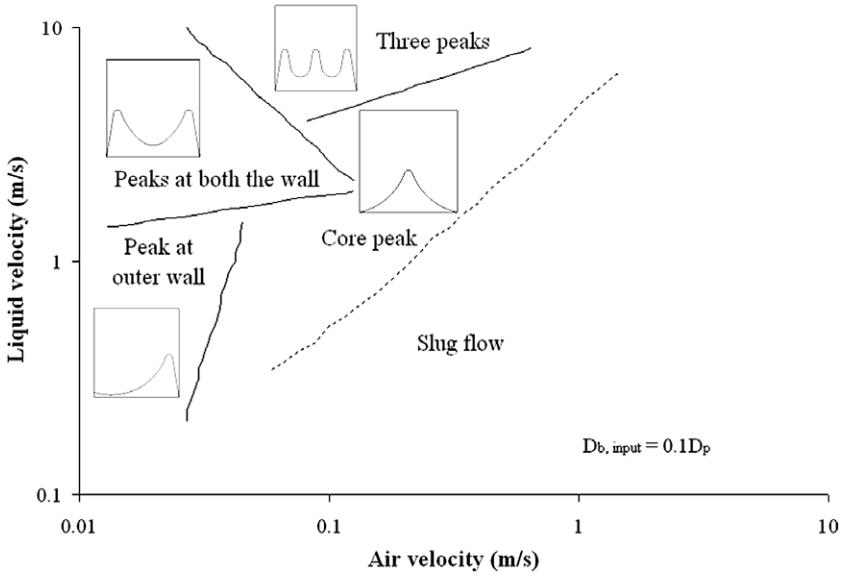

Fig. 7. A map in terms of flow velocities for different shapes of void distribution.

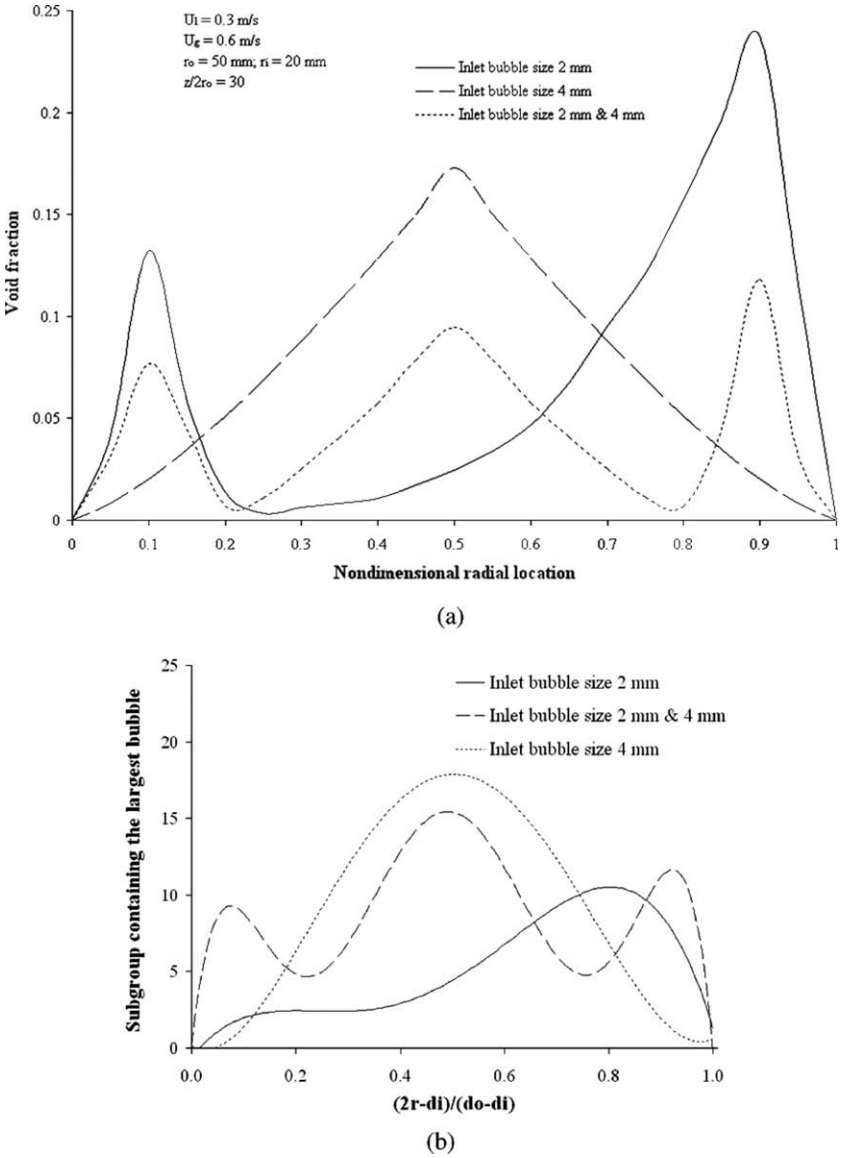

Fig. 8. Effect of different sized homogeneous and non-homogeneous bubble input in annular two phase flow over void fraction and bubble distribution.

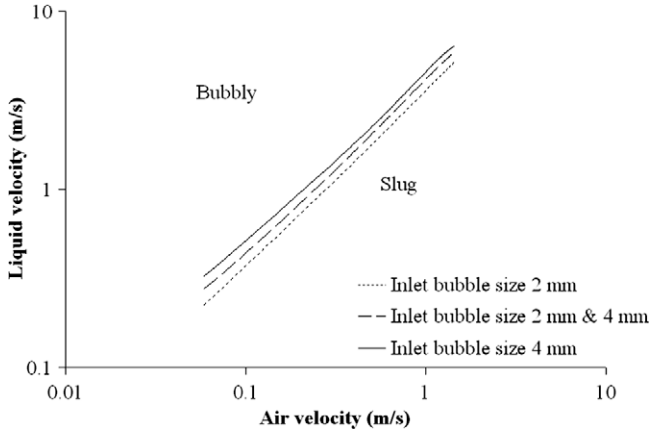

Fig. 9. Flow pattern map for bubbly flow to slug flow for input of 2 mm, 4 mm and a mixture of 2 mm and 4 mm bubbles at the inlet of annular geometry.

three flow pattern transition boundaries corresponding to 2 mm, 4 mm and simultaneous entry of 2 mm and 4 mm bubbles at the inlet plane are presented for a comparison. As the inlet bubble size increases slug flow appears at a lower liquid flow rate compared to smaller bubbles for a fixed air flow rate. Transition boundary for 2 mm bubble size at the entry shifts upward compared to the previous case. While both 2 mm and 4 mm diameter bubbles are introduced simultaneously transition line in the flow pattern map lies in between their individual transition boundaries. This evidently shows that transition boundaries are influenced by inlet bubble size. All the mechanistic models (Mishima and Ishii, 1984; Hasan and Kabir, 1992; Caetano et al., 1992) of flow regime transition failed to provide this information.

As mentioned earlier, the annular gap (defined by a non-dimensional term $r^* = (r_o - r_i)/r_o$) also influences the distribution of void fraction. Outcome of void distribution profile for various annular spacing is also studied using the present model. To evaluate the effect of wall forces on the dispersed phase the outer diameter of the annuli is kept constant and inner radius is varied in order to avail various spacing between the walls. At a liquid flow rate of 0.3 m/s and air flow rate of 0.1 m/s void distribution profile for various annular spacing is depicted in Fig. 10a. A sharp peek near the outer wall can be seen for narrow spacing of the annuli (r^* = 0.2 and 0.4). The height of the peak for r^* = 0.2 is higher compared to the peak at

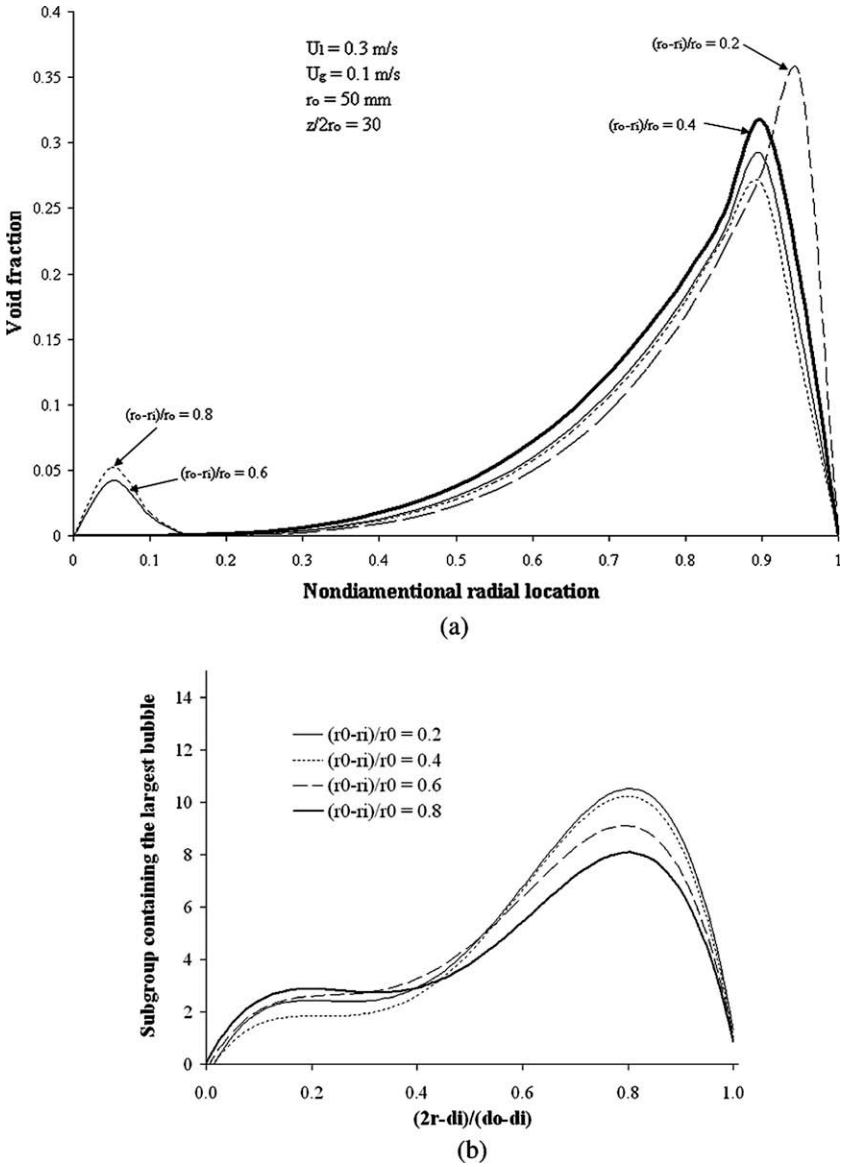

Fig. 10. Effect of annuli spacing over radial void and bubble distribution for air water two phase flow.

$r^* = 0.4$. But as r^* increase to 0.6 a small peak appears at the inner wall in addition to the peak at the outer wall. This trend continues for $r^* = 0.8$. Increase in the secondary peak height and decrease in the primary peak height can be seen as r^* changes from 0.6 to 0.8. This clearly shows that the effect of wall forces becomes significant in case of narrow spaced annuli. As the wall force diminishes with the channel spacing two peaks are formed at inner and outer periphery. Fig. 10b shows the largest bubble size present in the control volumes along the radial plane for various spacing of the annuli. It can be observed that the bubbles with the largest size are present near the outer wall. It also supports the outer wall peaking of the void distribution as shown in Fig. 10a. Largest possible bubble size decreases as the r^* decreases.

Flow pattern map for various gap widths of the annuli is presented in Fig. 11. The figure shows an interesting trend reversal for bubbly to slug transition. At the range of low air velocity transition to slug flow occurs at lower water flow rates with the increase in annular gap. As the wall force reduces with the annular gap the gas bubbles stay near the wall. This is not conducive for the formation of gas slugs. Only with the increase of gas flow rate or with the increase of the annular gap the void fraction in the core region increases giving rise to slug formation. On the other hand, at higher gas flow rate coalescence becomes predominant as the annular gap increases. This results in a transition to slug flow at lower water velocity.

3.4. Bubbly to dispersed bubbly transition

At higher liquid flow rate spheroidal bubbles break into smaller size and produce a homogeneous mixture of tiny air bubbles. This

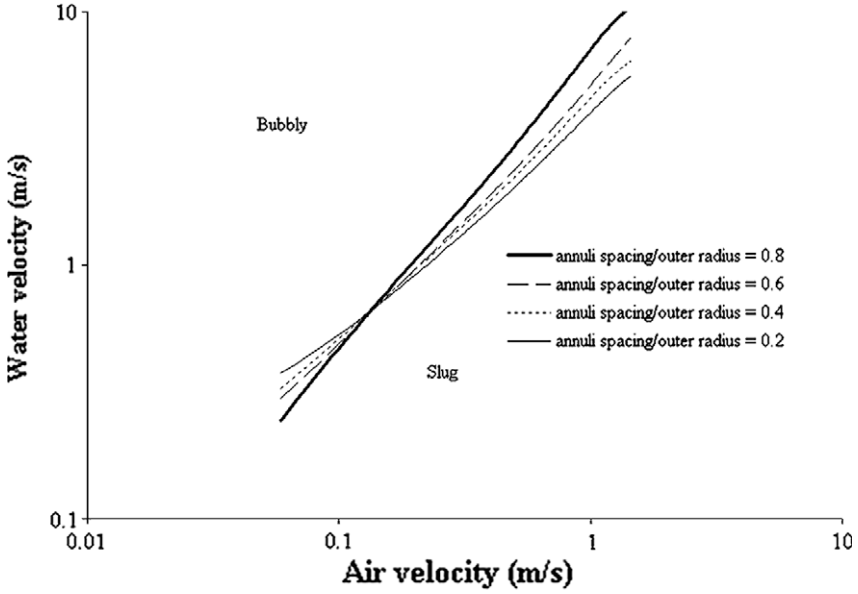

Fig. 11. Prediction of Bubbly to slug flow pattern map for various annuli spacing in air water two phase flow.

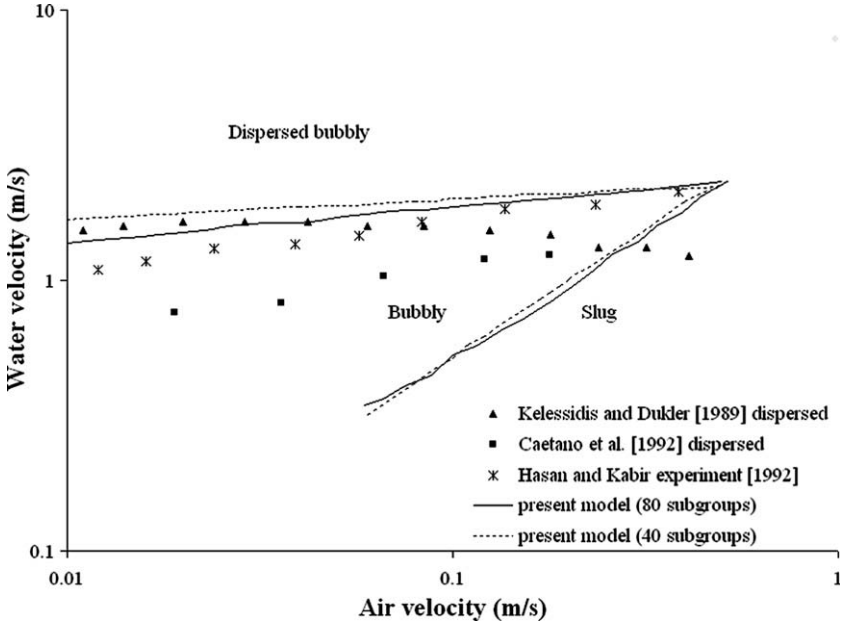

Fig. 12. Transitions of air water bubbly flow for different subgroup discretizations through annuli along with published experimental results.

is termed as dispersed bubbly flow (Taitel et al., 1980). At this condition the turbulence intensity is high enough to prevent the coalescence of the smaller bubbles. As a result, gas phase can remain dispersed in the form of spherical bubbles even at a high value of void fraction. The present model is extended to indicate the inception of dispersed bubbly flow by considering suitable closure relationship as the transition criteria. Equating turbulent kinetic energy and drop surface energy Hinze (1955) proposed a mechanism for estimating the maximum bubble size possible in dispersed bubbly flow for a fluid pair combination. The criterion is as follows:

$$\frac{D_{\text{surf}}}{D} = 0.55\left(\frac{\rho_l U_l^2 D}{\sigma}\right)^{-0.6}\left(\frac{\rho_m f}{\rho_l(1-\varepsilon)}\right)^{-0.4} \tag{29}$$

To investigate the bubbly to dispersed bubbly transition in the perspective of the present CFD model the simulations have been carried out at higher liquid flow rates. The evolution of bubble size has been closely monitored to check the criteria given in Eq. (29). The boundary for bubbly to dispersed bubbly transition, as obtained from the simulation, is depicted in Fig. 12. In the same figure the available experimental data and theoretical regime boundaries proposed by other researchers have also been depicted. Present model gives a better prediction of the experimental data of Hasan and Kabir (1992) throughout the domain in comparison with the data of Caetano et al. (1992) and Kelessidis and Dukler (1989). However, at lower air velocity there exists some deviation between the model prediction and experimental observation.

In the present model the possible span of bubble diameter is divided into 40 equal subgroups based on volume. As the volume of a bubble is a cubic function of its diameter, such a division generates a bubble population where the difference in the diameters between two subsequent subgroups is larger for small bubbles. This makes the distribution lopsided towards the large bubbles. In the simulation, daughter bubbles generated due to breakup are divided into its neighboring subgroups keeping its mass and number constant. The formation of small bubbles of intermediate size cannot be captured effectively in the lower range of diameter. The closure law for bubbly to dispersed bubbly transition depends directly on the spacing of bubble diameters of lower subgroups. To circumvent this, an alternate simulation has been made using 80 subgroups within the span of possible bubble volume. This minimizes the error in predicting the flow pattern due to birth of arbitrary sized bubbles caused by breakage.

Fig. 12 also depicts the transition curve for bubbly to dispersed bubbly flow inside annuli using 80 subgroups of bubble volume. It is evident that an increase in number of subgroups improves the prediction of regime boundary for bubbly to dispersed bubbly flow. It would be prudent to investigate whether introduction of more number of subgroups alters the bubbly slug regime boundary. In the same figure both the regime boundaries are plotted for 40 and 80 subgroups of bubble volume and it is observed that there is no significant change in bubbly slug transition in comparison to shift of regime boundary for bubbly-dispersed bubbly transition.

4. Conclusion

Transition from bubbly flow to the neighboring flow regimes during gas liquid two phase upflow through vertical annuli is modeled using the population balance equation coupled with a two-fluid model. Coalescence and breakup of bubbles due to the local hydrodynamics are taken care of to study the evolution of bubble size and generation of slug bubbles. Force arising from the interfacial interactions and wall lubrication are considered in the eulerian two fluid momentum equations as source terms.

Using the present model the local distribution of void fraction at a radial plane for different flow velocities has been studied inside the annuli. Outer wall peaking, both wall peaking, three peak and core peak can be separately identified for different ranges of phase velocities. Flow regime transition boundaries have also been generated from the numerical results that effectively show separate sub-regions for different distributions of the dispersed phase (Fig. 5). The regime boundary for bubbly flow to slug flow compares well with the reported experimental observations and theoretical predictions. Change of void fraction profile and flow pattern map has been analyzed for different inputs of bubble diameter at the inlet plane of the annular geometry. It has been seen that larger bubbles tries to be in the core of the annulus. These bubbles experience a further growth in size due to coalescence and gives rise to core peaking. With the increase of air flow rate core peaked bubbly flow transforms into slug flow (Fig. 7). Simultaneous entry of two different sized bubbles shows a mixed pattern reflecting the individual characteristics of the inlet bubble groups. It influences the transitions of the flow patterns also.

Further, the influence of the annular gap over void distribution has been studied. For narrow annular passages wall forces dominate over the interfacial forces prompting the bubbles to come close to the outer wall of the annular geometry. With an increase in the annular spacing interfacial forces become comparable to the wall forces. In the absence of any strong force, the bubble movement is neither biased towards the core nor towards the wall. At low air flow rate the appearance of slug bubbles in wide annuli is detected at lower water flow rate. On the contrary, at higher flow rate a relatively low liquid flow rate gives rise to slug bubble formation in narrow annuli due to the increased intrinsic vibration of the bubbles. It is important to note that the present simulation have been made for annular dimensions common in engineering practice and for which published experimental results and theoretical predictions are available. In case of extremely narrow annuli the dominating forces may be different from those considered. As a result all together different flow regimes may be obtained (Nakoryakov et al., 1992). Simulation of two phase flow through narrow annuli could be a separate topic of research.

Simulation at a high liquid flow rate shows a decrease in the bubble size even for increasing air flow rates. Using the criteria proposed by Hinze (1955) the transition to dispersed bubbly flow could be predicted readily. The prediction matches well with the experimental data of Caetano et al. (1992) at lower air flow rate and that of Hasan and Kabir (1992) for higher flow rate. An improvement in the prediction is observed when the number of bubble subgroup is increased from 40 to 80. However, such a change has only a marginal effect on the transition boundary from bubbly to slug flow.

References

Anderson, T.B., Jackson, R.A., 1967. Fluid mechanical description of fluidized beds: equations of motion. Industrial and Engineering Chemistry Fundamentals 6, 527–539.

Bunner, B., Tryggvason, G., 2002. Dynamics of homogeneous bubbly flows: Part 1. Rise velocity and microstructure of the bubbles. Journal of Fluid Mechanics 466, 17–52.

Caetano, E.F., 1984. Two-phase flow in a vertical annulus. TUFFP Report, University of Tulsa, OK.

Caetano, E.F., Shoham, O., Brill, J.P., 1992. Upward vertical two-phase flow through an annulus, Part I: single phase friction factor, Taylor bubble rise velocity and flow pattern prediction. In: Proceedings of 4th International Conference on Multiphase Flow, Nice, France.

Carrica, P.M., Clausse, A.A., 1993. Mathematical description of the critical heat flux as nonlinear dynamic instability. In: Gouesbet, G., Berlemont, A. (Eds.), Instabilities in Multiphase Flow. Plenum Press, New York.

Chesters, A.K., 1991. The modelling of coalescence processes in fluid–liquid dispersions: a review of current understanding. Transactions of the Institute of Chemical Engineers 69, 259–270.

Cheung, S.C.P., Yeoh, G.H., Tu, J.Y., 2006. On the modelling of population balance in isothermal vertical bubbly flows—average bubble number density approach. Chemical Engineering Processing 46, 742–756.

Chisholm, D., 1973. Pressure gradient due to friction during the flow of evaporating two phase mixtures in smooth tubes and channel. International Journal of Heat and Mass Transfer 16, 347–358.

Coulaloglou, C.A., Tavlarides, L.L., 1977. Description of interaction processes in agitated liquid–liquid dispersions. Chemical Engineering Science 32, 1289–1297.

Das, G., Das, P.K., Purohit, N.K., Mitra, A.K., 1999. Flow pattern transition during gas liquid upflow through vertical concentric annuli—part I: experimental investigations. ASME Journal of Fluids Engineering 121, 895–901.

Das, A.K., Das, P.K., Thome, J.R., 2009a. Transition of bubbly flow in vertical tubes: new criteria through CFD simulation. ASME Journal of Fluids Engineering 131 (9), 091303.1–091303.12.

Das, A.K., Das, P.K., Thome, J.R., 2009b. Transition of bubbly flow in vertical tubes: effect of bubble size and tube diameter. ASME Journal of Fluids Engineering 131 (9), 091304.1–091304.6.

Drahos, J., Zahradnik, J., Puncochar, M., Fialova, M., Bradka, F., 1991. Effect on operating conditions on the characteristics of the pressure fluctuations in a bubble column. Chemical Engineering Processing 29, 107–115.

Eckert, S., Gerbeth, G., Melnikov, V.I., 2003. Velocity measurements at high temperatures by ultrasound droplet velocimetry using an acoustic wave guide. Experiments in fluids 35, 381–388.

Ekberg, N.P., Ghiaasiaan, S.M., Abdel-Khalik, S.I., Yoda, M., Jeter, S.M., 1999. Gas–liquid two-phase flow in narrow horizontal annuli. Nuclear Engineering and Design 192, 59–80.

Frank, T., Shi, J., Burns, A.D., 2004. Validation of Eulerian multiphase flow models for nuclear safety application. In: Proceedings of 3rd International Symposium on Two-Phase Modelling and Experimentation, Pisa, Italy.

Fu, X.Y., Ishii, M., 2003. Two-group interfacial area transport in vertical air–water flow I. Mechanistic model. Nuclear Engineering Design 219, 143–168.

Hasan, A.R., Kabir, C.S., 1992. Two-phase flow in vertical and inclined annuli. International Journal of Multiphase Flow 18 (2), 279–293.

Hibiki, T., Situ, R., Mi, Y., Ishii, M., 2003. Local flow measurements of vertical upward bubbly flow in an annulus. International Journal of Heat and Mass Transfer 46, 1479–1496.

Hinze, J., 1955. Turbulence. McGrawhill, New York, USA.

Ioannou, K., Hu, B., Matar, O.K., Hewitt, G.F., Angeli, P., 2004. Phase inversion in dispersed liquid–liquid pipe flows. In: Proceedings of Fifth International Conference on Multiphase Flow, Yokohama, Japan.

Ishii, M., 1975. Thermo-Fluid Dynamic Theory of Two-Phase Flow. Eyrolles, Paris.

Ishii, M., Mishima, K., 1984. Two-fluid model and hydrodynamic constitutive relations. Nuclear Engineering and Design 82, 107–126.

Kelessidis, V.C., Dukler, A.E., 1989. Modeling flow pattern transitions for upward gas–liquid flow in vertical concentric and eccentric annuli. International Journal of Multiphase Flow 15 (2), 173–191.

Kostoglou, M., Karabelas, A.J., 1998. Theoretical analysis of steady state particle size distribution in limited breakage process. Journal of Physics A: Mathematical and General 31, 8905–8921.

Kostoglou, M., Karabelas, A.J., 2006. Towards a unified framework for the derivation of breakage functions based on the statistical theory of turbulence. Chemical Engineering Science 60, 6584–6595.

Kostoglou, M., Dovas, S., Karabelas, A.J., 1997. On the steady state size distribution of dispersions in breakage processes. Chemical Engineering Science 52, 1285–1299.

Krussenberg, A.K., Prasser, H.M., Schaffrath, A., 1999. A new criterion for the bubble slug transition in vertical tubes. In: Proceedings of 9th International Topical Meeting on Nuclear Reactor Thermal Hydraulics (NURETH-9), San Francisco, CA, USA.

Kumar, S., Ramkrishna, D., 1996. On the solution of population balance equations by discretization—I. A fixed pivot technique. Chemical Engineering Science 51 (8), 1311–1332.

Lienhard IV, J.H., Lienhard V, J.H., 2004. A Heat Transfer Textbook. Phlogiston Press, Cambridge.

Liu, T.J., Bankoff, S.G., 1993. Structure of air–water bubbly flow in a vertical pipe. II: void fraction, bubble velocity and bubble size distribution. Journal of Heat Transfer 36, 1061–1072.

Liu, T.J., Wang, S.J., 2001. Optimization of local and area-averaged interfacial area concentration correlations in twophase bubbly flow. In: Proceedings of Fourth International Conference on Multiphase Flow, New Orleans, USA.

Lopez de Bertodano, M., 1998. Two fluid model for two phase turbulent jet. Nuclear Engineering Design 179, 65–74.

Lovick, J., 2004. Horizontal oil–water flows in the dual continuous flow regime. Ph.D. thesis, University College London, London, UK.

Lucas, D., Krepper, E., Prasser, H.M., 2005. Development of co-current air–water flow in a vertical pipe. International Journal of Multiphase Flow 31, 1304–1328.

Lucas, D., Krepper, E., Prasser, H.M., 2007. Use of models for lift, wall and turbulent dispersion forces acting on bubbles for poly-disperse flows. Chemical Engineering Science 62 (15), 4146–4157.

Luo, H., Svendsen, H.F., 1996. Theoretical model for drop and bubble breakup in turbulent dispersions. AIChE Journal 42, 1225–1233.

Mishima, K., Ishii, M., 1984. Flow regime transition criteria for upward two-phase flow in vertical tubes. International Journal of Heat and Mass Transfer 27, 723–737.

Nakoryakov, V.E., Kuznetsov, V.V., Vitovsky, O.V., 1992. Experimental investigation of upward gas–liquid flow in a vertical narrow annulus. International Journal of Multiphase Flow 18 (3), 313–326.

Osamasali, S.I., Chang, J.S., 1988. Two-phase flow regime transition in a horizontal pipe and annulus flow under gas–liquid two-phase flow. ASME Fluid Engineering Division 72, 63–69.

Prince, M.J., Blanch, H.E., 1990. Bubble coalescence and break-up in air-sparged bubble columns. AIChE Journal 36, 1485–1499.

Richter, H.J., 1983. Separated two-phase flow model: application to critical two phase flow. International Journal of Multiphase Flow 9 (5), 511–530.

Sadatomi, M., Sato, Y., Saruwatari, S., 1982. Two-phase flow in vertical noncircular channels. International Journal of Multiphase Flow 8 (6), 641–655.

Serizawa, A., Kataoka, I., Michiyoshi, I., 1975. Turbulence structure of air–water bubbly flow—II. Local properties. International Journal of Multiphase Flow 2, 235–246.

Sorour, M.M., El-Beshbeeshy, M.S., 1986. Void fraction and pressure fluctuations of bubbly flow in a vertical annular channel. Experiments in Fluids 4, 163–170.

Sun, X., Kuran, S., Ishii, M., 2004. Cap bubbly-to-slug flow regime transition in a vertical annulus. Experiments in Fluids 37, 458–464.

Taitel, Y., Bornea, D., Dukler, A.E., 1980. Modelling flow pattern transitions for steady upward gas–liquid flow in vertical tubes. AIChE Journal 26 (3), 345–354.

Tomiyama, A., Nakahara, Y., Adachi, Y., Hosokawa, S., 2003. Shapes and rising velocities of single bubbles rising through an inner subchannel. Journal of Nuclear Science and Technology 40, 136–142.

Tsouris, C., Tavlarides, L.L., 1994. Breakage and coalescence models for drops in turbulent dispersions. AIChE Journal 40, 395–406.

Wallis, G.B., 1969. One Dimensional Two-Phase Flow. McGraw-Hill, New York.

Wang, T., Wang, J., Jin, J., 2003. A novel theoretical breakup kernel function for bubbles/droplets in a turbulent flow. Chemical Engineering Science 58, 4629–4637.

Wongwises, S., Pipathattakul, M., 2006. Flow pattern, pressure drop and void fraction of two-phase gas–liquid flow in an inclined narrow annular channel. Experimental Thermal and Fluid Science 30, 345–354.

Wu, Q., Kim, S., Ishii, M., Beus, S.G., 1998. One-group interfacial area transport in vertical bubbly flow. International Journal of Heat and Mass Transfer 41, 1103–1112.

Yeoh, G.H., Tu, J.Y., 2004. Population balance modelling for bubbly flows with heat and mass transfer. Chemical Engineering Science 59, 3125–3139.

Yeoh, G.H., Tu, J.Y., 2006. Two-fluid and population balance models for subcooled boiling flow. Applied Mathematical Modelling 30, 1370–1391.

Zuber, N., Findlay, J., 1969. Average volumetric concentration in two-phase flow systems. Transactions on ASME Journal of Heat Transfer 87, 453–468.

Zun, I., 1990. The mechanism of bubble non-homogeneous distribution in two-phase shear flow. Nuclear Engineering and Design 118, 155–162.